Egyptian Journal of Chemistry

http://ejchem.journals.ekb.eg/

Computer-Aided Design of Lead Flavonoid Compounds Targeting VP35 for Marburg Virus Treatment

Saba Beigh[1, *]

[1]*Department of Public Health, Faculty of Applied Medical Sciences, Albaha University, Al-Baha 65431, Saudi Arabia*

Abstract

Numerous multidisciplinary strategies aimed at expediting and reducing the cost of drug development have captured the interest of researchers. The primary objectives of this study involve the identification of target proteins and the selection of a lead drug for combating the Marburg Virus. In pursuit of these goals, the VP35 pharmacological target (PDB ID: 4gh9) was discerned through a comprehensive literature review. The three-dimensional structure was obtained from the Protein Data Bank. Utilizing Auto Dock Vina within Pyrx, druggable flavonoids were subjected to molecular docking. The interactions between these chemical compounds and their respective target proteins were scrutinized employing BIOVIA Discovery Studio. Furthermore, the stability of protein-inhibitor complexes in a physiological milieu was assessed through Molecular Dynamics Simulation (MD simulation) using Desmond. Our investigation reveals that the primary compounds CID969516 and CID5280445 exhibit inhibitory effects, thereby impeding the functionality of the virus. This discovery holds significant implications for broader research efforts and may culminate in the development of novel medications. The adept repurposing of these chemicals has demonstrated efficiency as inhibitors, accompanied by a reduction in adverse effects and heightened efficacy.

Keywords: Marburg Virus; Molecular Dynamic Simulation; Flavonoids; Therapeutic Regimen

1. Introduction

The Marburg virus is a lethal zoonotic infectious agent known to cause Marburg virus disease (MVD), with a mortality ratio of 88% [1]. Belonging to the Filoviridae family, Marburg virus induces hemorrhagic fever in both primates and other non-primates. Bats of the African and Egyptian rousette species serve as the reservoir hosts for the Marburg virus [2]. The virus has experienced outbreaks in various regions, including Guinea, Uganda, Africa, USA, Netherlands, Germany, Soviet Union, and Kenya [3]. Characterized as negative-sense, filamentous, and snail-like in structure, the Marburg virus exhibits a rod or six-shaped appearance [4]. Transmission of the virus from one individual to others occurs through direct contact with bodily fluids such as blood, tears, serum, and breast milk [5]. The incubation period for Marburg virus infection ranges from 2 to 15 days [6]. The Marburg virus genome encodes seven structures of proteins, known as ORF (open reading frame) structures. These viral proteins include VP24, VP-30, VP-35, VP-40, Glycoprotein, Large protein, and Nucleoprotein [7] VP24, produced from six genes, plays a crucial role in the assembly of viral particles during infections [8.] VP24 is involved both before and after replication but does not impact genome replication. VP30 proteins, akin to VP30 in the Ebola Virus, play a major role in transcription [9]. VP35 acts as an interferon (IFN) antagonist, impeding antiviral protein activity and is vital in blocking host antiviral responses [10]. VP40 is involved in virion synthesis and slows down gene expression [11]. The Glycoprotein (GP) presents a single surface that functions as an immune evasion mechanism [12]. Nucleoprotein (NP) plays a significant role in budding and transcription and serves as the central protein pivot for the virus.[13] The Large Protein (LP) is the focal point of the polymerase complex, exhibiting enzymatic characteristics during viral replication [14]. The viral protein VP35 is indispensable for several crucial processes in the Marburg virus life cycle. It plays a key role in the assembly of the nucleocapsid, facilitates virus replication, and is involved in the

*Corresponding author e-mail: sbeigh@bu.edu.sa (Saba Beigh)
Receive Date: 14 November 2023, Revise Date: 05 February 2024, Accept Date: 03 April 2024
DOI: 10.21608/ejchem.2024.248327.8867

transcription of the viral genome. Beyond these functions, VP35 assumes a critical role in immunosuppressing the host. VP35's significance extends to its ability to bind to viral double-stranded RNA (dsRNA), resulting in the antagonism of the type I interferon (IFN) response [13]. This binding event inhibits the phosphorylation and activation of interferon regulatory factor 3 (IRF-3) and suppresses RNA silencing mechanisms. Moreover, the interaction with dsRNA serves to conceal VP35 from host factors, likely preventing its degradation. Notably, VP35 has garnered attention as a potential drug target for Marburg virus (MARV), supported by various studies demonstrating its effectiveness in treating Ebola virus infections [14]. The multifaceted roles of VP35 in the viral life cycle and its immunomodulatory functions underscore its significance as a potential therapeutic target for antiviral drug development. The increasing popularity of natural remedies for the treatment of brain disorders worldwide is attributed to their lack of negative side effects. These compounds, originating from the flavonoid class, play diverse roles in various biological processes. Flavonoids, characterized as low molecular weight phenolic compounds, are gaining recognition due to their broad spectrum of health benefits. They exhibit a range of biological properties, including neuroprotective effects, making them valuable in nutraceutical, pharmaceutical, medicinal, and cosmetic applications. The versatility of flavonoids and their positive impact on neurological health contribute to their growing popularity as natural agents for therapeutic interventions.

This study employed computational methodologies to discern potential compounds with anti-Marburg activity. Natural compounds were subjected to virtual screening to evaluate their efficacy against the target protein, VP35 from the Marburg virus. The resulting docked complexes underwent comprehensive analysis, incorporating considerations of binding energies and interactions to identify the most promising candidates. Subsequently, selected compounds underwent molecular dynamics simulations, with myricetin serving as the control in a comparative study. Additionally, the MM/GBSA technique was applied to determine the free binding energies of the selected compounds. Cumulatively, these findings illuminate promising candidates capable of effectively targeting VP35 of the Marburg virus, presenting encouraging prospects for the development of therapeutic interventions against this disease.

2. Materials and Methods

2.1. Target retrieval from RCSB PDB and preparation

Utilizing the distinctive Protein Data Bank (PDB) identifier 4gh9 for the VP35 protein of the Marburg virus, three-dimensional structures of the targeted proteins were procured from the RCSB PDB. The Protein Data Bank serves as a versatile online repository encompassing a myriad of macromolecules, including proteins, DNA, and RNA, rendering it an invaluable resource [15,16]. Employing MODELLER, loop refinement techniques were applied to enhance the precision of the protein structures. Subsequently, crystal structures of the proteins underwent optimization and minimization procedures through RAMPAGE and Swiss PDB Viewer. The assessment of the protein structure quality was conducted, with RAMPAGE generating a Ramachandran Plot that exhibited a lack of discrepancies. This plot not only affirmed the structural integrity but also delineated the amino acid residues situated within the preferred, permitted, or outlier zones, furnishing additional insights. Moreover, binding sites on the protein targets were forecasted using CASTp (Computed Atlas of Surface Topography of Proteins) 3.0. CASTp, recognized for its reliability, presents a comprehensive method for scrutinizing and quantifying protein surface topography, thereby facilitating the identification of potential binding sites [17-20].

2.2. Molecular Docking

From the available literature, a substantial selection of pharmacologically relevant flavonoids was meticulously chosen. Employing Auto Dock Vina, a sophisticated molecular docking program [21, 22], we subjected these chosen compounds to a meticulous screening process. This involved docking the selected compounds with specific protein receptors to scrutinize and quantify their interactions, as well as to evaluate their binding affinities with the designated target proteins. To facilitate this assessment, PyMOL was utilized to generate complex files that encompassed both the receptor and ligand structures. Subsequently, BIOVIA Discovery Studio was employed for the comprehensive analysis and visualization of two-dimensional protein-ligand interactions. This analytical approach not only shed light on the intricate interplay between the compounds and the receptor proteins but also enhanced our understanding of the nuanced dynamics governing these interactions [23, 24].

2.3. Lead Identification

An exhaustive ADMET (Absorption, Distribution, Metabolism, Excretion, and Toxicity) analysis of the selected medications was conducted using the

Qikprop methodology. This approach streamlined the evaluation of a diverse array of pharmacokinetic and pharmacodynamic properties associated with the compounds, aiding in the determination of their viability as potential therapeutic candidates. Within this comprehensive analysis, a specific chemical entity emerged, exhibiting intriguing characteristics when juxtaposed with docking binding affinity data and the outcomes of the ADMET investigation. To substantiate the binding and stability of this identified molecule with the target protein within a physiologically relevant context, we extended our investigations through additional biophysical and biochemical experiments. These endeavours provided valuable insights into the compound's therapeutic potential and its efficacy in interacting with the target protein under conditions that closely mimic the biochemical milieu of the human body. The amalgamation of binding affinity, ADMET analysis, and extensive experimental validations contributes to a more nuanced understanding of the compound's promise as a therapeutic option.

2.4. Molecular Dynamics Simulation

A comprehensive exploration of the dynamic behavior of the molecular system was undertaken through 100 nanosecond molecular dynamics simulations, employing the Desmond program. This in-depth analysis delved into the intricate movements and interactions of individual atoms over a specified time frame, elucidating the ligand-binding behavior within the active site of the target protein. The initiation of molecular dynamics (MD) simulations followed a crucial preliminary step—protein-ligand docking, which provided an initial static depiction of the ligand's binding within the target protein. To refine and optimize the ligand-receptor combination, Maestro's Protein Preparation Wizard was deployed, addressing system intricacies and rectifying any missing residues. The System Builder tool facilitated the holistic construction of the entire system. The OPLS_2005 force field and the TIP3P (Intermolecular Interaction Potential 3 Points Transferable) fluid model were employed, maintaining the temperature at 310 K and the pressure at 1 atm. A sodium chloride concentration of 0.15 M was simulated, with neutralizing ions incorporated to ensure system neutrality, mimicking physiological conditions. The models underwent initial equilibration, with frequent checkpoints for evaluation established, capturing data at 100 ps intervals, before the commencement of the modeling itself [29, 30]. This dynamic modeling technique not only enables the observation of interactions and changes between molecules over time but also furnishes a profound understanding of how the system functions within a dynamic and fluid environment [25-28].

3. Results and Discussion

The three-dimensional structure of the receptor was derived from the Protein Data Bank (PDB). The VP35 protein, with a molecular weight of 65.36 kilodaltons, exhibits an asymmetric-C1 symmetry, signifying a lack of rotational symmetry. The VP35 complex demonstrates a hetero 3-mer stoichiometry, composed of three unique subunits identified as A1, B1, and C1. In simpler terms, this information conveys that the VP35 protein possesses a specific total weight, and its 3D structure is sourced from a database. The absence of rotational symmetry implies that its structural elements lack repetition or symmetry, and the protein forms a complex with three distinct subunits, designated as A1, B1, and C1. This detailed characterization is crucial for a comprehensive understanding of the VP35 protein's structural attributes.

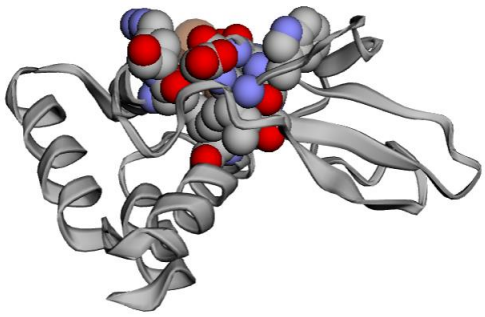

Figure 1: This figure illustrates the three-dimensional structure of a protein obtained from the Protein Data Bank under the entry 4gh9.

The depicted image encapsulates the final protein structure post-loop reduction and optimization, accentuating the predicted binding site. Remarkably, the structure exhibits a remarkable conformity to desired structural norms, boasting an exceptional overall quality score of 99%. In essence, Figure 1 serves as a visual representation of the three-dimensional configuration of a protein sourced from PDB entry 4gh9. The highlighted region in the image delineates the section of the protein anticipated to engage with other molecules, showcasing the structural outcome following loop modifications and minimization. With a precision rate of 99%, the construction attains an exceedingly high level of quality, aligning seamlessly with the sought-after structural attributes—a facet particularly pertinent for researchers investigating the protein's function and potential interactions.

Table 1 elucidates the binding affinities and ADMET analyses for the top 5 leads. Notably, compounds CID969516 and CID5280445 emerge as the most potent for the protein target post-lead identification. Figure 2 provides a visual representation of the two-dimensional

interactions of these high-performing compounds. Offering a comprehensive overview of the key compounds' characteristics, Table 1 serves as a valuable resource. To delve deeper into the understanding of these intriguing chemicals, a 100-nanosecond molecular dynamics (MD) simulation was conducted for the protein targets in conjunction with the most efficacious compounds. The MD trajectories underwent rigorous analyses, encompassing evaluations of protein-ligand interactions and parameters such as root mean square deviation (RMSD) and root mean square fluctuation (RMSF). AutoDock Vina facilitated docking investigations for the top hits. In tandem, an ADMET research initiative, employing tools like QikProp and pkCSM, scrutinized the pharmacokinetic and safety profiles of these substances. Table 1 underscores the selection of the top 5 compounds for further scrutiny based on their ADMET and docking outcomes. This comprehensive approach not only identifies potential therapeutic candidates with favorable pharmacophore matches but also underscores their promising biological activity, embodying a holistic methodology in drug discovery. Table 1 displays the molecular weight of the compounds in the "mol_MW" column. The molecular weight range that is considered acceptable is 130.0 to 725.0. The predicted number of hydrogen bonds the solute may establish with water molecules is shown by the variable "donorHB". The predicted number of hydrogen bonds the solute might accept from water molecules in an aquatic environment is indicated by the symbol "accptHB". Because this number is an average over several setups, it may not always be an integer. Generally speaking, it should lie between 0.0 and 6.0. The estimated octanol/water partition coefficient, or "QPlogPo/w" value, indicates how hydrophobic a molecule is. Generally speaking, this number should fall between -2.0 and 6.5. For "QPlogHERG," the inhibitory concentration (IC50) for HERG K+ channel blockage is shown. When it comes to possible negative consequences, values less than five are deemed worrying. The Caco-2 cell permeability prediction, which gauges how quickly a substance may cross the gut-blood barrier, is represented by the "QPPCaco" number. Values above 500 indicate great permeability, whereas values between 0 and 25 indicate inadequate permeability. "QPlogBB" is a measure of the predicted blood/brain separation ratio that sheds light on a compound's potential blood-brain barrier crossing capabilities. When using QikProp to anticipate oral medications,
the range usually falls between -3.0 and -1.2. This value aids in determining if a substance has the ability to impact the central nervous system. Finally, information on a compound's binding to human serum albumin may be found using "QPlogKhsa" and "Human serum albumin binding predictions". The predicted range of these values, which represent the degree of interaction between the chemical and this blood protein, is often between -1.5 and 1.5. Understanding the compound's pharmacokinetics and its therapeutic uses depends heavily on these factors.

Table 1: Table showing binding affinity and ADMET analysis of top compounds.

CID	mol_MW	SASA	donorHB	accptHB	QPlogPo/w	QPlogHERG	QPPCaco	QPlogBB	QPlogKhsa	Binding Affinity
969516	368.385	701.733	2	7	2.735	-6.273	151.758	-2.256	-0.026	-6.5
5280445	286.24	500.018	3	4.5	0.941	-5.022	45.023	-1.91	-0.205	-6.3
5280343	302.24	514.002	4	5.25	0.362	-5.035	20	-2.352	-0.354	-6.2
5280443	270.241	489.281	2	3.75	1.624	-5.125	124.496	-1.411	-0.043	-6.2
5280863	286.24	503.264	3	4.5	1.036	-5.14	55.32	-1.843	-0.201	-6.1

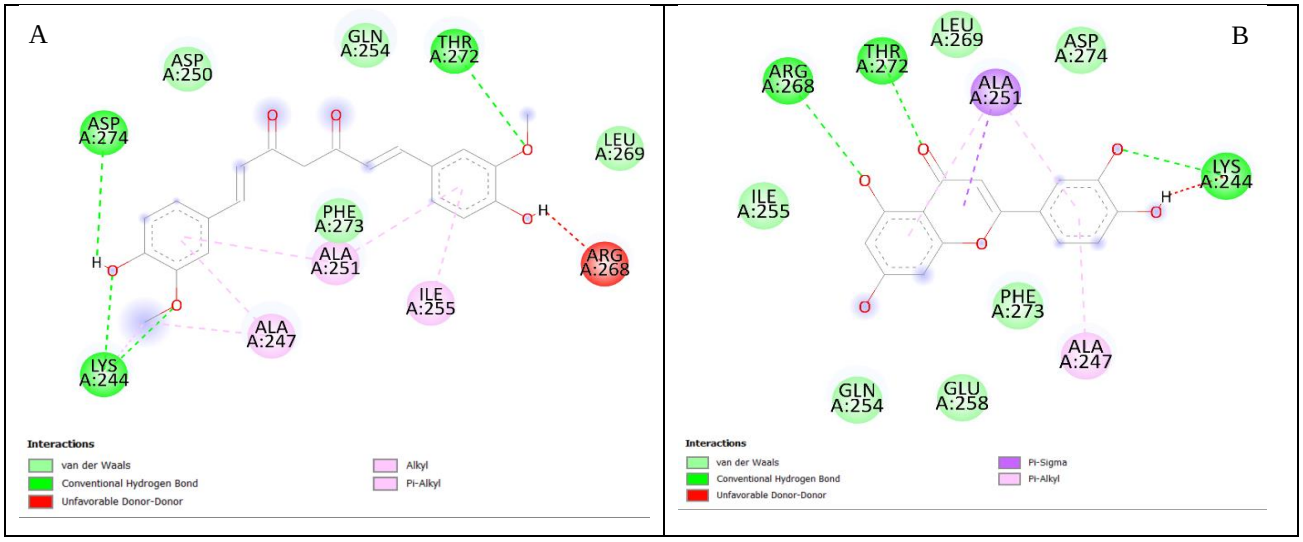

Figure 2: Interactions of lead compound with protein target showing interacting residues. A: CID969516, B: CID5280445

Following the discovery of the lead compound, two particular compounds, CID969516 and CID5280445, were shown to be the most effective of all the compounds under investigation. The 2D interactions of this high-performing chemical are illustrated in Figure 2, which offers information on its molecular interactions with the target protein. The salient characteristics of this fascinating compound that are critical to its potential as a therapeutic candidate are presented in Table 1. To have a deeper understanding of the interactions and behaviour of this optimal chemical combination with the protein target, a 100 nanosecond molecular dynamics simulation was performed. This simulation was performed using Desmond software, and the resulting trajectories were analysed afterwards.

As part of the inquiry, values for root-mean-square-deviation (RMSD) and root-mean-square-fluctuation (RMSF) were calculated. While RMSD provides information on the stability and structural changes of the complex over time, RMSF illustrates the flexibility of the complex's numerous components during the simulation. A thorough examination of the material's interactions with the protein provided insight into how the material adheres
to and interacts with the target during the simulation. Through the provision of informative information on the chemical's behaviour and potential as a therapeutic candidate, this comprehensive analysis facilitates the evaluation of the compound's stability, binding qualities, and suitability for further development.

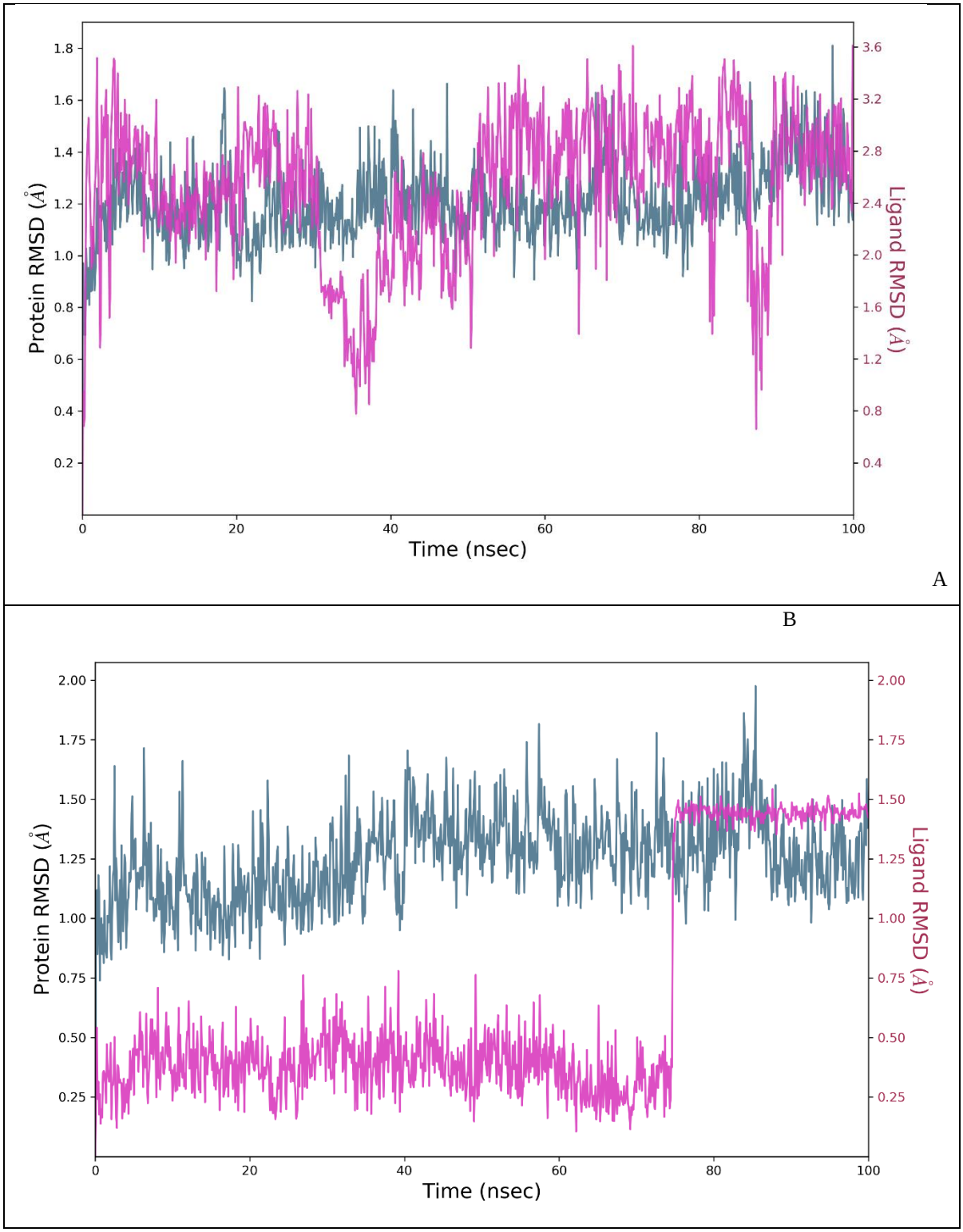

Figure 3: Showing how, over time, the distance between the C-alpha atoms of proteins and the lead molecule has changed. Over the duration of the simulation, the RMSD of the lead molecule is shown in pink, whilst the RMSD of the protein target is shown in grey. *A: CID*969516-6gh9, *B: CID*5280445-6gh9

.

Figure 3 provides a graphical representation of the Root Mean Square Deviation (RMSD) values for the C-alpha atoms in proteins bound to the ligand. RMSD serves as a metric to quantify the extent of deviation in a protein's structure from its initial state throughout a molecular dynamic's simulation. Analysis of the RMSD figure reveals that the complexed protein structure in this simulation achieved a stable state at approximately 10 nanoseconds. This stability is corroborated by the RMSD values plateauing and consistently remaining within a range of approximately 1.5 Angstroms for the duration of the simulation. Such sustained structural stability is indicative of a positive outcome, suggesting that the protein retained its overall structure over the course of the simulation. Additionally, the protein structure represented by the PDB ID 6gh9 exhibited a gradual increase in RMSD values, implying structural changes over time. However, these changes occurred incrementally with relatively minor fluctuations. This gradual and limited structural evolution supports the notion that the protein maintained robust structural integrity throughout the simulation.

Furthermore, the Ligands Fit to Protein, an indicator of how well a ligand molecule fits into a protein's binding site, remained constant during the simulation. While the ligand's RMSD values fluctuated over time, signifying movement or conformational changes, equilibrium was reached without substantial alterations in the ligand's RMSD. In summary, the RMSD plot demonstrates the attainment of a stable state in the protein-ligand complexes. Despite some oscillations, both the ligand and the protein preserved their structural integrity during the simulation, affirming the stability of the protein structure and advocating for its suitability for further in-depth study. Figure 4 displays the Root Mean Square Fluctuation (RMSF) values for a protein linked to a ligand. These RMSF values show how much, during a molecular dynamic's simulation, certain amino acid residues in the protein structure deviate from their usual locations. The analysis of the molecular dynamics trajectories demonstrates that residues with larger RMSF plot peaks are typically located in flexible regions, such as loops or the protein's N- and C-terminal ends. This implies that there is more structural variety and dynamic activity in these regions. The stability of the ligand binding to the protein is ascertained by analysing the RMSF values of the residues in the ligand-binding site. Reduced RMSF values indicate minimal fluctuations in the ligand-protein interaction throughout the simulation for these binding site residues. Figure 5 describes the secondary structural elements (SSE) that were present in the protein during the simulation. It provides a graphic representation of the distribution of beta strands and alpha helices across the protein structure, illustrating the distribution in connection to the residue index. Plotting the SSE against the residue index in the graph illustrates the location of these structural elements inside the protein. Based on the statistical analysis, these constituents account for about 42.84 percent of the secondary structure of complex CID969516-6gh9. More precisely, alpha-helices account for around 32.82 percent of secondary structural components, whereas beta-strands account for approximately 10.02 percent. Together, these components account for approximately 44.74 percent of the secondary structure of the protein in complex CID969516-6gh9. More precisely, around 10.98 percent of the secondary structural components are composed of beta-strands, whereas approximately 33.77 percent are composed of alpha-helices. Figure 4, which provides a summary of the flexibility of individual residues within the protein, displays more flexible or dynamic regions of the protein based on higher RMSF values. The binding site's reduced RMSF values indicate that ligand-protein interactions are stable. Figure 6 shows the relative amounts and distribution of beta-strands and alpha-helices inside the protein's secondary structure.

This study provides crucial information on the stability of the protein's interactions with the ligand and its simulated behaviour.

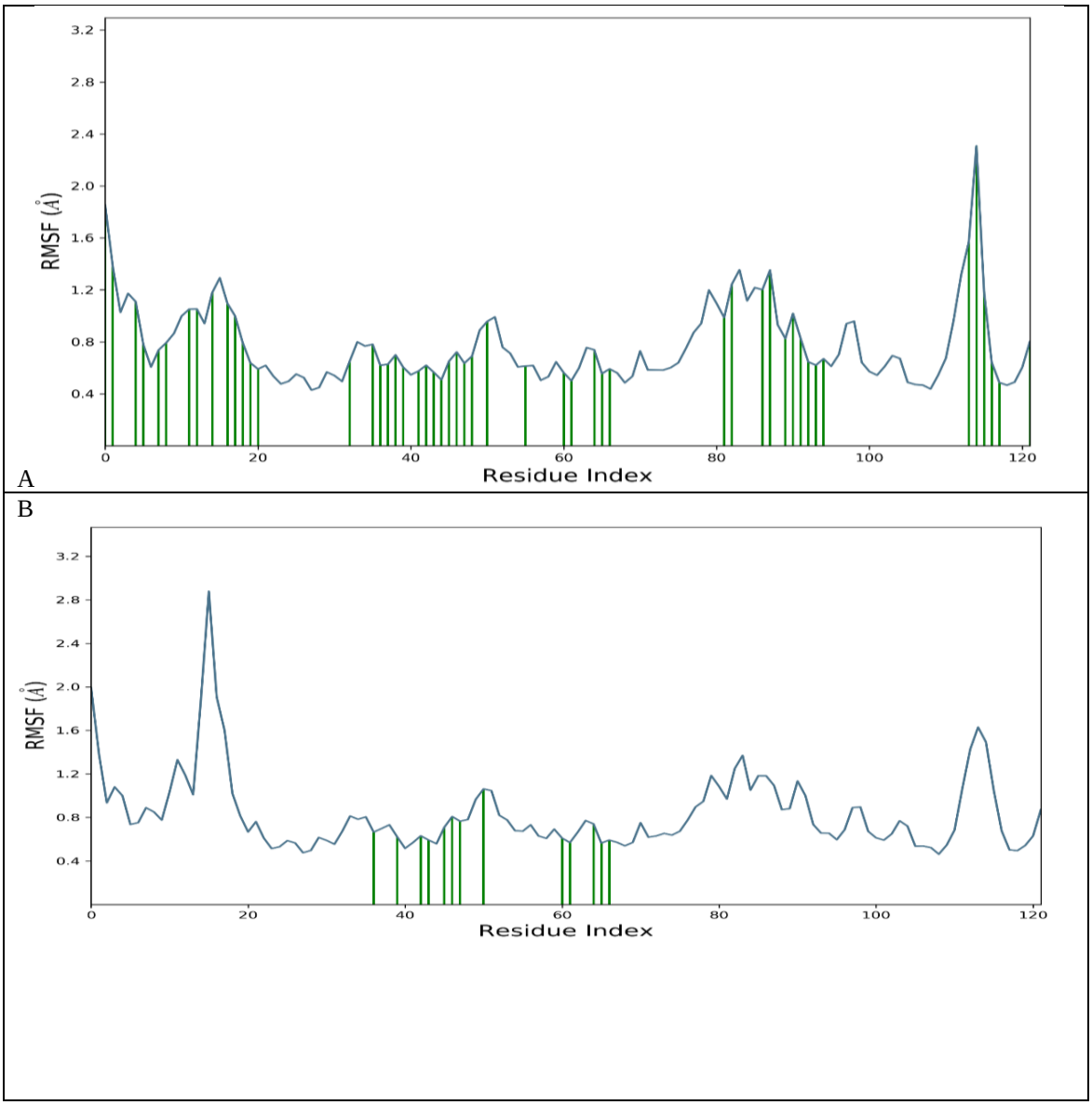

Figure 4: Root Mean Square Fluctuation (RMSF) of a protein in a ligand complex, measured in terms of residues. *A: CID*969516-6gh9, *B: CID*5280445-6gh9

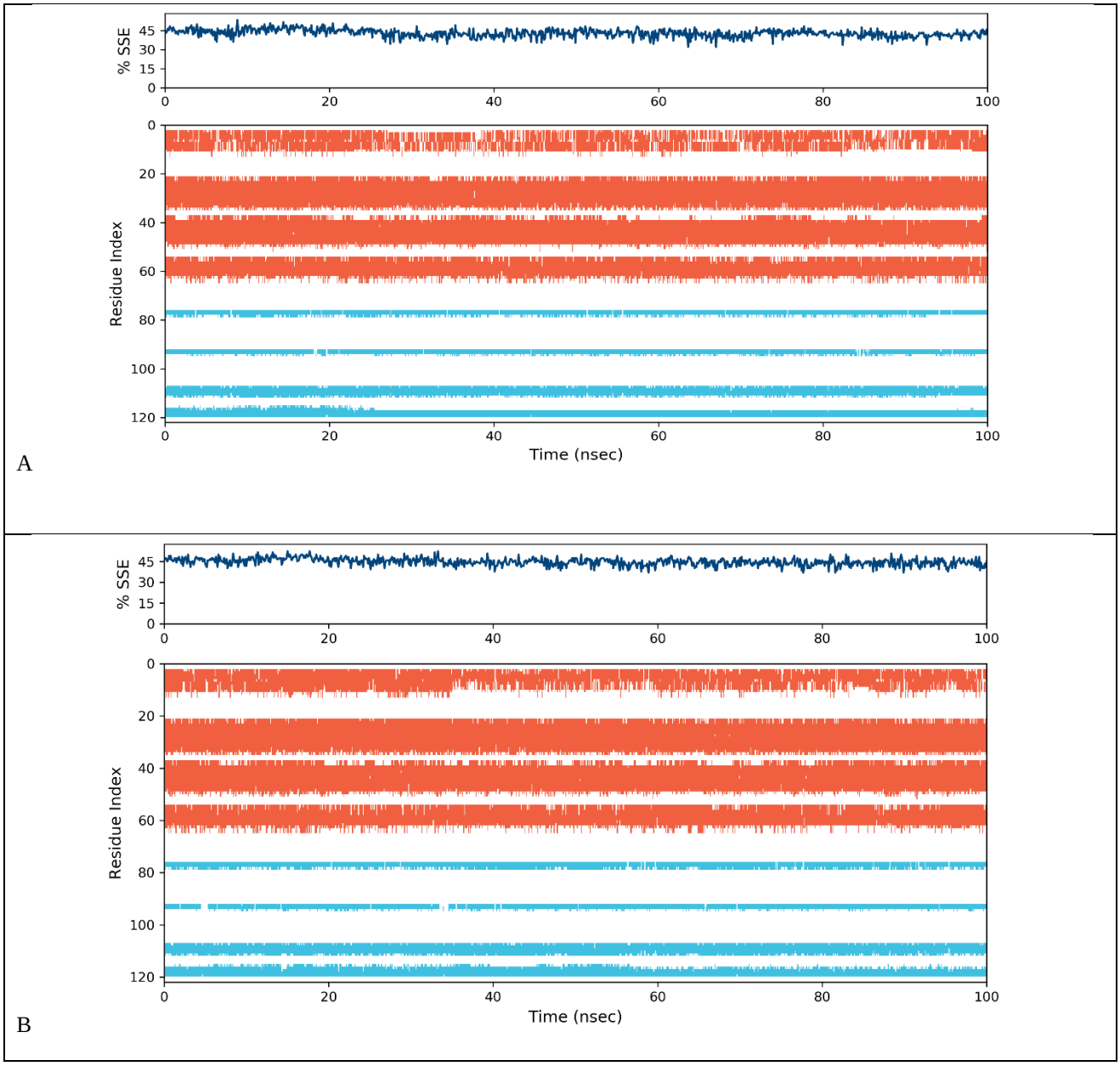

Figure 5: Illustrating the distribution of elements of secondary protein structure within protein-ligand complexes in relation to the position of each residue. Specifically, alpha helices are depicted as red columns, and beta strands are represented by blue columns. *A: CID*969516-6gh9, *B: CID*5280445-6gh9

The primary form of interaction that takes place between the protein and the ligand during the molecular dynamics (MD) simulation is represented by hydrogen bonds, as seen in Figure 6. These hydrogen bonds are essential for the ligand's stability and protein binding. In particular, hydrogen bonding plays a major role in the interactions between certain amino acids and the ligand. Notable amino acids are ASP_250 and ASP_274 in the CID5280445-6gh9 complex and HIS_220, ASN_224, and LEU_249 in the CID969516-6gh9 complex. These amino acids are especially sensitive to hydrogen bonding interactions and are necessary for the ligand to bind to the protein efficiently. The dynamic changes in the contacts and interactions between ligands and proteins during the experiment are depicted in the timeline in the chart below Figure 6. This timeline allows researchers to monitor the timing and manner of these crucial interactions during the simulation, offering valuable information into the dynamics and stability of the ligand-protein complex.

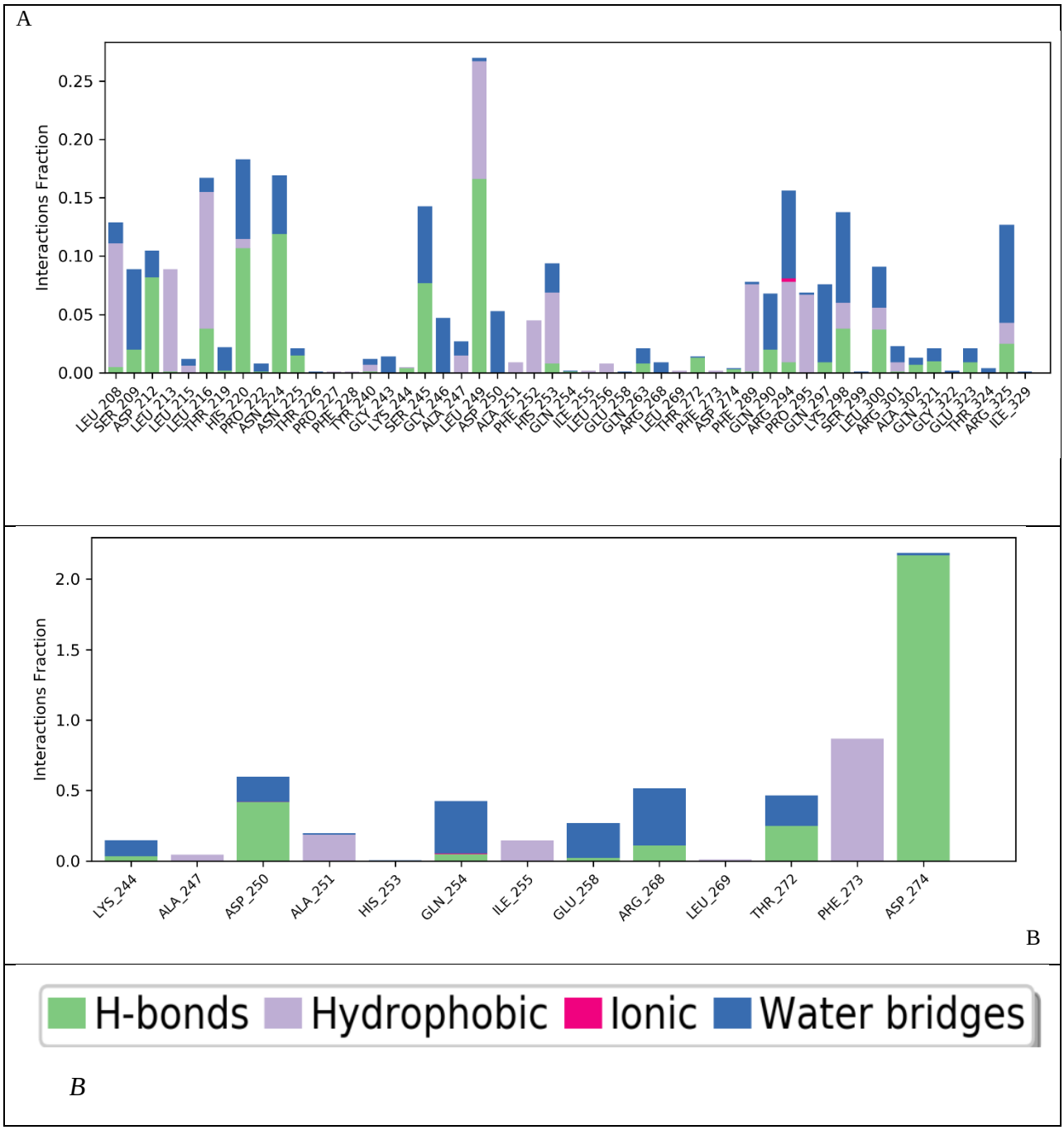

Figure 6: Protein-ligand contact h*istogram* throughout trajectory. *A: CID*969516-6gh9, *B: CID*5280445-6gh9

To sum up, Figure 6 illustrates the significance of hydrogen bonds in the interactions that occur between the protein and ligand. It highlights certain amino acids whose role in binding is dependent on hydrogen bonding. The timeline display, which offers a dynamic view on the evolution of these interactions, facilitates a deeper understanding of the complex's behaviour during the MD simulation.

4. Conclusions

In the realm of drug development, the pursuit of interdisciplinary methodologies has been a driving force to expedite processes and mitigate overall costs. The primary objective of this study was to identify specific target proteins associated with the Marburg virus, laying the foundation for the selection of a lead drug candidate. To counteract the impact of the lead

chemical on the viral protein, we sought substances possessing this quality. Among the identified candidates, CID969516 and CID5280445 emerged as two potential natural inhibitors. These inhibitors demonstrated a significant reduction in the activity of protein 4gh9 at its receptor location. Our rationale posits that these compounds may serve as a foundational platform for the development of a medication that selectively targets the Marburg virus while preserving the integrity of other biological processes. These findings hold immense promise for the scientific community, potentially contributing to the eventual creation of a novel treatment for this viral disease.

5. Author Contributions: Dr. Saba Beigh conceived the manuscript, authored it, and conducted the review. Dr. Saba has thoroughly read and provided approval for the published version of the manuscript.

6. Funding: This research received no external funding.

7. Institutional Review Board Statement: Not applicable

8. Informed Consent Statement: Not applicable

9. Data Availability Statement: The authors confirm that the data supporting the study's findings are included in the article as supplementary files

10. Conflicts of Interest: The authors declare no conflict of interest

11. References

1. Alsaady, I. M.; Bajrai, L.H.; Alandijany, T.A.; Gattan, H.S.; El-Daly, M.M.; Altwaim, S.A.; Alqawas, R.T.; Dwivedi, V.D.; Azhar, E.I. Cheminformatics Strategies Unlock Marburg Virus VP35 Inhibitors from Natural Compound Library. *Viruses*, 2023, *15*(8), 1739. doi: 10.3390/v15081739.

2. Mavrakis, M.; Kolesnikova, L.;Schoehn, G.; Becker, S.; Ruigrok, R.W. Morphology of Marburg virus NP-RNA. *Virology*. 2002,296, 300-307. doi: 10.1006/viro.2002.1433.

3. Pervin, T.; Oany, A.R. Vaccinomics approach for scheming potential epitope-based peptide vaccine by targeting l-protein of Marburg virus. *In Silico Pharmacol.* 2021, 9, 21. doi: 10.1007/s40203-021-00080-3.

4. Geisbert, T. W.; Hensley, L. E.; Geisbert, J. B.; Leung, A.; Johnson, J. C.; Grolla, A.; Feldmann, H. Postexposure treatment of Marburg virus infection. *Emerg. Infect. Dis.* 2010, 16, 1119–1122. doi: 10.3201/eid1607.100159

5. Kortepeter, M.G.; Dierberg, K.; Shenoy, E.S.; Cieslak, T.J. Medical Countermeasures Working Group of the National Ebola Training and Education Center's (NETEC) Special Pathogens Research Network (SPRN). Marburg virus disease: A summary for clinicians. *Int J Infect Dis*. 2020;99, 233-242. doi: 10.1016/j.ijid.2020.07.042.

6. Nakayama, E.; Saijo, M. Animal models for Ebola and Marburg virus infections. *Front Microbiol*. 2013,4,267. doi: 10.3389/fmicb.2013.00267.

7. Zhang, L.; Li, Q.; Liu, Q.; Huang, W.; Nie, J.; Wang, Y. A bioluminescent imaging mouse model for Marburg virus based on a pseudovirus system. *Hum. Vaccin. Immunother*. 2017,13,1811-1817. doi: 10.1080/21645515.2017.1325050.

8. Srivastava, S., Sharma, D., Kumar, S., Sharma, A., Rijal, R., Asija, A., Adhikari, S., Rustagi, S., Sah, S., Al-Qaim, Z. H., Bashyal, P., Mohanty, A., Barboza, J. J., Rodriguez-Morales, A. J., Sah, R. Emergence of Marburg virus: a global perspective on fatal outbreaks and clinical challenges. *Front Microbiol*. 2023,14,1239079. doi: 10.3389/fmicb.2023.1239079.

9. Tigabu, B., Ramanathan, P., Ivanov, A., Lin, X., Ilinykh, P. A., Parry, C. S., Freiberg, A. N., Nekhai, S., Bukreyev, A. Phosphorylated VP30 of Marburg Virus Is a Repressor of Transcription. *J Virol*. 2018;92(21):e00426-18. doi: 10.1128/JVI.00426-18.

10. Liu, B., Dong, S., Li, G., Wang, W., Liu, X., Wang, Y., Yang, C., Rao, Z., Guo, Y. *Structural Insight into Nucleoprotein Conformation Change Chaperoned by VP35 Peptide in Marburg Virus. J Virol*. 2017;91(16):e00825-17. doi: 10.1128/JVI.00825-17.

11. O'Donnell, K. L., Feldmann, F., Kaza, B., Clancy, C. S., Hanley, P. W., Fletcher, P., & Marzi, A. Rapid protection of nonhuman primates against Marburg virus disease using a single low-dose VSV-based vaccine. *EBioMedicine*. 2023,89, 104463. doi: 10.1016/j.ebiom.2023.104463

12. Schiffman, Z., Garnett, L., Tran, K. N., Cao, W., He, S., Emeterio, K., Tierney, K., Azaransky, K., Strong, J. E.,Banadyga, L. The inability of Marburg virus to cause disease in ferrets is not solely linked to the virus glycoprotein. *J Infect Dis*. 2023;jiad206. doi: 10.1093/infdis/jiad206.

13. Sibomana, O.; Kubwimana, E. First-ever Marburg virus disease outbreak in Equatorial Guinea and Tanzania: An imminent crisis in West and East Africa. *Immun Inflamm Dis*. 2023,11, e980. doi: 10.1002/iid3.980.

14. Albaqami, F. F., Altharawi, A., Althurwi, H. N., Alharthy, K. M., Qasim, M., Muhseen, Z. T.,Tahir Ul Qamar, M. Computational Modeling and Evaluation of Potential mRNA and Peptide-Based Vaccine against Marburg Virus (MARV) to Provide

Immune Protection against Hemorrhagic Fever. *Biomed Res Int*. 2023;2023:5560605. doi: 10.1155/2023/5560605

15. Amatya, P., Wagner, N., Chen, G., Luthra, P., Shi, L., Borek, D., Pavlenco, A., Rohrs, H., Basler, C. F., Sidhu, S. S., Gross, M. L., Leung, D. W. Inhibition of Marburg Virus RNA Synthesis by a Synthetic Anti-VP35 Antibody. *ACS Infect Dis*. 2019;5(8):1385-1396. doi: 10.1021/acsinfecdis.9b00091.

16. Berman, H. M., Westbrook, J., Feng, Z., Gilliland, G., Bhat, T. N., Weissig, H., Shindyalov, I. N., & Bourne, P. E. *The Protein Data Bank. Nucleic Acids Res*. 2000;28(1):235-242. doi: 10.1093/nar/28.1.235.

17. Eswar, N., Webb, B., Marti-Renom, M. A., Madhusudhan, M. S., Eramian, D., Shen, M. Y., Pieper, U., Sali, A. Comparative protein structure modeling using Modeller. Curr Protoc Bioinformatics. 2006;Chapter 5:Unit-5.6.

18. Guex N, Peitsch MC. SWISS-MODEL and the Swiss-PdbViewer: an environment for comparative protein modeling. *Electrophoresis*, *18*(15), 2714–2723. doi: 10.1002/elps.1150181505

19. Ho, B. K.,Brasseur, R. The Ramachandran plots of glycine and pre-proline. *BMC Struct Biol*. 2005;5:14. doi: 10.1186/1472-6807-5-14

20. Tian, W., Chen, C., Lei, X., Zhao, J., Liang, J. (2018). CASTp 3.0: computed atlas of surface topography of proteins. *Nucleic Acids Res*. 2018;46(W1):W363-W367. doi: 10.1093/nar/gky473.

21. Kandeel, M., Iqbal, M. N., Ali, I., Malik, S., Malik, A.,Sehgal, S. A. Comprehensive in silico analyses of flavonoids elucidating the drug properties against kidney disease by targeting AIM2.*PLoS One*. 2023;18(5):e0285965. doi: 10.1371/journal.pone.0285965.

22. Trott, O.; Olson, A.J. AutoDock Vina: improving the speed and accuracy of docking with a new scoring function, efficient optimization, and multithreading. *J Comput Chem*. 2010;31(2):455-461. doi: 10.1002/jcc.21334.

23. Mura, C., McCrimmon, C. M., Vertrees, J., Sawaya, M. R. An introduction to biomolecular graphics. *PLoS Comput Biol*. 2010;6(8):e1000918.

24. Systemes, D. BIOVIA Discovery Studio. San Diego, 2022. doi: 10.1371/journal.pcbi.1000918.

25. Bowers, K.J.a.C., David E. and Xu, Huafeng and Dror, Ron O. and Eastwood, Michael P. and Gregersen, Brent A. and Klepeis, John L. and Kolossvary, Istvan and Moraes, Mark A. and Sacerdoti, Federico D. and Salmon, John K. and Shan, Yibing and Shaw, David E., Scalable Algorithms for Molecular Dynamics Simulations on Commodity Clusters. SC '06: Proceedings of the 2006 ACM/IEEE Conference on Supercomputing. 2006: IEEE. 43-43.

26. Ferreira LG, Dos Santos RN, Oliva G, Andricopulo AD. Molecular docking and structure-based drug design strategies. Molecular docking and structure-based drug design strategies. *Molecules (Basel, Switzerland)*, *20*(7), 13384–13421. doi: 10.3390/molecules200713384.

27. Hildebrand, P. W., Rose, A. S.,Tiemann, J. K. S. Bringing Molecular Dynamics Simulation Data into View. *Trends Biochem Sci*. 2019;44(11):902-913. doi: 10.1016/j.tibs.2019.06.004

28. Rasheed, M. A., Iqbal, M. N., Saddick, S., Ali, I., Khan, F. S., Kanwal, S., Ahmed, D., Ibrahim, M., Afzal, U.,Awais, M. Identification of Lead Compounds against Scm (fms10) in Enterococcus faecium Using Computer Aided Drug Designing. *Life (Basel)*. 2021;11(2):77. doi: 10.3390/life11020077.

29. Shivakumar, D., Williams, J., Wu, Y., Damm, W., Shelley, J., Sherman, W. Prediction of Absolute Solvation Free Energies using Molecular Dynamics Free Energy Perturbation and the OPLS Force Field. *J Chem Theory Comput*. 2010;6(5):1509-1519. doi: 10.1021/ct900587b.

30. Grant, B. J., Skjaerven, L., Yao, X. Q. The Bio3D packages for structural bioinformatics. *Protein Sci*. 2021;30(1):20-30. doi: 10.1002/pro.3923.